Optical Transition Radiation Interferometry for A0 Photoinjector

G. Kazakevich* (BINP),
H. Edwards, R. Fliller, V. Lebedev, S. Nagaitsev, J. Santucci, R. Thurman-Keup (FNAL)
P. Piot (FNAL/NIU),
J. Li (Synopsys Inc.)
R. Tikhoplav (UCLA).

Introduction

A charged particle passing through the boundary of two medias with different permittivity values generates Transition Radiation (TR), [1]. The TR is caused by a variation of the particle electric field with variation of the permittivity. The TR for relativistic particles has a wide spectrum with a significant portion in the optical range. The Optical Transition Radiation (OTR) is widely used for a beam profile monitoring and measurements of a beam size. Moreover, OTR can be used to characterize the energy, energy spread and transverse angles in the beam by employing the interference of the OTR from two thin films [2] inserted in the beam trajectory. This method has been applied in number of works [3-5] demonstrating high results and good coincidence in measurements and calculations. In this paper we present and discuss in details a simulation of the interference pattern in several experimental setups. We consider the main optical effects, for diagnostics for the beam properties at A0 Photoinjector and the ILC module test area (NML) in a wide range of electron beam energy.

In this paper, we first derive the OTR intensity formula for a single film at 90 degrees to the beam, then for two films at normal incidence, and finally with films at 45 degree incidence to the beam. The last section illustrates application with beam parameters like those at the A0 Photoinjector (electron energy 15 MeV).

OTR caused by relativistic electrons passing through thin transparent film.

First we consider the OTR generated in a single thin transparent dielectric film. The forward TR generated by transition of an electron through the boundary vacuum-media at normal incidence has the following intensity distribution [6]:

$$I_\varepsilon(\omega,\theta_\varepsilon) = \frac{e^2\beta^2\sqrt{\varepsilon}\cdot\sin^2\theta_\varepsilon\cdot\cos^2\theta_\varepsilon}{\pi^2 c\cdot(1-\beta^2\varepsilon\cdot\cos^2\theta_\varepsilon)^2}\times$$
$$\times\left|\frac{(\varepsilon-1)\cdot\left(1-\beta^2\varepsilon-\beta\sqrt{1-\varepsilon\cdot\sin^2\theta_\varepsilon}\right)}{\left(1-\beta\sqrt{1-\varepsilon\cdot\sin^2\theta_\varepsilon}\right)\cdot\left(\cos\theta_\varepsilon+\sqrt{\varepsilon}\cdot\sqrt{1-\varepsilon\cdot\sin^2\theta_\varepsilon}\right)}\right|^2 \qquad (1)$$

In the expression: θ_ε is the angle between the electron velocity and the wave vector of the OTR photon in the film having the frequency ω. The permittivity of the film is $\varepsilon = \varepsilon(\omega)$. At $\cos(\theta_\varepsilon) = 1/\beta\cdot\sqrt{\varepsilon} = \cos(\theta_{Ch})$ the expression has a pole caused by Cherenkov radiation, which like the TR is a result of coherent response of the media to the passage of the electron. For relativistic electrons and dielectric films used in OTR techniques: $\beta\to 1$ and $\sqrt{\varepsilon}$ is in range of 1.5-1.7; so the $\theta_{Ch} > \theta_r$, where $\theta_r = a\sin(1/\sqrt{\varepsilon})$ is the total internal reflection angle.

---

* Current affiliation: FNAL, Batavia, IL

Due to this, at small angles of observation and micrometers-thick film one can neglect contribution of the Cherenkov radiation in the light radiated forward along the electron passage through the dielectric film. Note that we also do not consider the distortion of the field of the electron in media caused by Cherenkov radiation.

In optical range $\omega << \gamma\omega_p$, where: $\omega_p = \sqrt{\frac{4\pi \cdot n_e \cdot e^2}{m_e}}$ is the plasma frequency, γ is the relativistic factor, n_e, e and m_e are the electron density, charge of the electron and mass of the electron, respectively, and $\omega_p \sim 3 \cdot 10^{16}\ s^{-1}$ for transparent dielectrics traditionally used in OTR techniques, the dependence of ε and consequently of the last term in (1) on the frequency ω is quite weak, [7]. Due to this for the forward OTR photons, relativistic electrons and small observation angles, $\theta_\varepsilon \approx \gamma^{-1} = \sqrt{1-\beta^2}$, one can write: $I(\omega, \theta_\varepsilon) \approx I(\theta_\varepsilon)$.

Consider OTR generated in a transparent film with thickness d at normal incidence of the electron. First we discuss the OTR generated at the film first boundary. Correspondingly to (1) the initial forward OTR generated at **I** boundary has an amplitude of $\sqrt{I(\theta_\varepsilon)}$. The wave reflected from the second boundary (**II**) has the amplitude of $\approx r \cdot \sqrt{I(\theta_\varepsilon)}$. Here: $r = \left|\frac{\sqrt{\varepsilon}-1}{\sqrt{\varepsilon}+1}\right| = \left|\frac{n-1}{n+1}\right|$ is the reflection coefficient at normal incidence; n is the refraction index of the film. From the energy conservation it follows that the amplitude of the first transmitted forward wave is: $\approx \sqrt{1-r^2} \cdot \sqrt{I(\theta_\varepsilon)}$, see Fig. 1. Consequently, the second transmitted forward wave amplitude is: $\approx r^2 \cdot \sqrt{1-r^2} \cdot \sqrt{I(\theta_\varepsilon)}$, and so on. Note that θ is the refraction angle for the boundary film-vacuum; the value is determined by the expression: $\sin\theta = n \sin\theta_\varepsilon$.

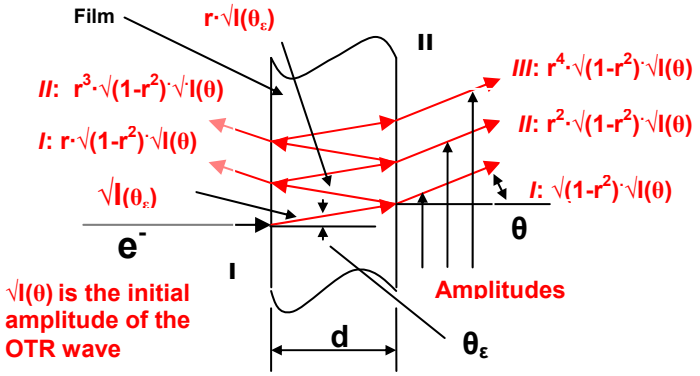

Fig.1. Forward OTR propagation caused by transition of the electron through boundary **I** of the transparent film. The numbers ***I, II***, and so on (in red) mark transmitted forward (or transmitted backward) waves of the original and first, second, and so on reflected OTR amplitudes.

Similarly, in the backward direction one obtains amplitudes for the first reflected wave: $\approx r \cdot \sqrt{1-r^2}\sqrt{I(\theta_\varepsilon)}$, for the second reflected wave: $\approx r^3\sqrt{1-r^2}\sqrt{I(\theta_\varepsilon)}$, and so on.

Summing the waves with their relative phases (without consideration of absorption of the OTR in the film), and considering refraction of the light on the boundary film-

vacuum, one obtains the amplitude in the forward wave generated by transition through the first boundary:

$$F_I(\theta) = \sqrt{1-r^2} \cdot \sqrt{I(\theta_\varepsilon)} \cdot e^{i\varphi(\theta_\varepsilon)} \cdot \left(1 + r^2 \cdot e^{2i\varphi(\theta_\varepsilon)} + \ldots\right) = \frac{\sqrt{1-r^2} \cdot \sqrt{I(\theta_\varepsilon)}}{1 - r^2 \cdot e^{2i\varphi(\theta_\varepsilon)}} \cdot \exp\left(i \cdot \varphi(\theta_\varepsilon(\theta))\right). \quad (2)$$

Here: $\varphi(\theta_\varepsilon) = \frac{2\pi \cdot d \cdot n}{\lambda \cdot \cos\theta_\varepsilon}$, and λ is the wavelength of the detected OTR. Note that the phases in the all waves are considered relative to the reference plane in which the fronts of the interfering waves coincide; the angle θ_ε is transformed into angle θ as was noted above.

Additional forward OTR interfering with $F_I(\theta)$ is generated by the electron transition through the **II** boundary of the film. The electron crossing the boundary of dielectric-vacuum generates the forward OTR with the intensity distribution described as, [8]:

$$I_{II}(\omega,\theta) = \frac{e^2\beta^2 \sin^2(\theta) \cdot \cos^2(\theta)}{\pi^2 c[1-\beta^2\cos^2(\theta)]^2} \cdot \left| \frac{(\varepsilon - 1) \cdot (1 - \beta^2 - \beta\sqrt{\varepsilon - \sin^2(\theta)})}{(1 - \beta\sqrt{\varepsilon - \sin^2(\theta)}) \cdot (\varepsilon\cos(\theta) + \sqrt{\varepsilon - \sin^2(\theta)})} \right|^2 . \quad (3)$$

The last term in this expression also depends weakly on the frequency, so in the optical range far from the plasma frequency one can write: $I_{II}(\omega,\theta) \approx I_{II}(\theta)$.

So the amplitude of the forward wave generated on the **II** boundary considering the phase is expressed as:

$$F_{II}(\theta) \cong \sqrt{I_{II}(\theta)} \cdot \exp\left(i \cdot \frac{2\pi \cdot d}{\lambda} \cdot \left(\frac{1}{\beta\cos\theta_e} + (\tan\theta_\varepsilon(\theta) - \tan\theta_e)\sin\theta \right) \right). \quad (4)$$

Here: θ_e is the projection of the average angle of the multiple scattering of the electrons in the film. The phase term in the OTR wave includes the phase caused by a pass of the electron through the film and a term caused by propagation of the wave front in vacuum to the reference plane.

The backward intensity distribution of OTR generated by a transition of the electron through the **II** boundary looks as (1), but with reversed sign of β [6]. The distribution similarly to one expressed by (1) gives the Cherenkov radiation at $\cos\theta = \frac{1}{\beta \cdot \sqrt{\varepsilon}}$ but does not show the OTR at small angles to the incidence, so we do not consider that.

Expressing the amplitude of the superposition of the forward waves as: $F_T(\theta) = F_I(\theta) + F_{II}(\theta)$ we calculated the total intensity in forward wave generated by electrons passing through transparent dielectric film at normal incidence to the beam axis using following formula:

$$I_T(\theta) = \left|F_T(\theta)\right|^2 . \quad (5)$$

Dielectric films traditionally used in the OTRI techniques are the polymer transparent films as Mylar, nitrocellulose, etc. Result of the $I_T(\theta)$ calculation for various thickness of Mylar film *(n=1.65)* are plotted in Fig. 2 in relative units. The scale of the units is the same for all presented plots.

In the figure various curves are plotted for comparison with $I_T(\theta)$: $I_{I-II}(\theta)$ -resulting intensity of the forward waves from **I** and **II** boundaries without consideration of the multiple reflected OTR waves, $I_I(\theta) = \left|F_I(\theta)\right|^2$ -intensity in forward wave generated by pass through **I** boundary considering multiple reflection in the film and $I_{II}(\theta) = \left|F_{II}(\theta)\right|^2$ -

intensity in forward wave generated by pass through **II** boundary. All these curves were calculated for non-scattered electrons.

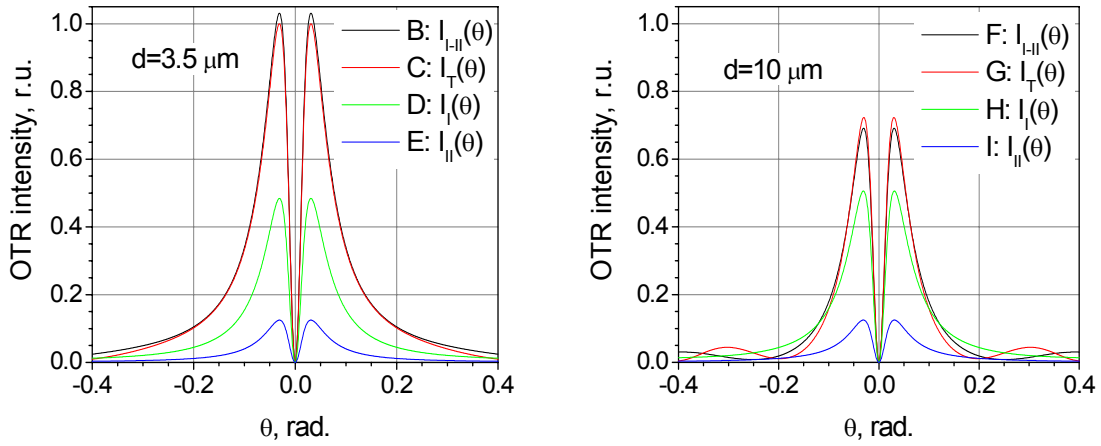

Fig. 2. Angular distribution (in arbitrary units) of the intensity of the OTR caused by 16 MeV electron passing through single 3.5 μm- or 10 μm- Mylar film at λ = 0.632 μm. (Definition of the different curves is given above).

The curves demonstrate absence of the fringes at small angles comparable with $1/\gamma$ and small thickness. This is explained by small phase shift of the OTR in thin film. Increase of the film thickness leads to appearance of the fringes first of all at bigger angles. Variation in the OTR intensity vs. the film thickness is caused by interference of photons radiated at both boundaries of the film. From calculations follows that peak values of $I_I(\theta)$ including contribution of the multiple reflected OTR are varied (because of the interference) vs. variation of the film thickness in the range of ≈ 23% for considered thickness range of the Mylar films.

Note that the (1) and (3) expressions are applicable for all media, including metals. For those the $\varepsilon(\omega)$ contents a big imaginary part, so in metals, [9]:

$$\varepsilon_m(\omega) \approx i \cdot 4\pi \frac{\sigma}{\omega}. \qquad (6)$$

Here: σ is the media electrical conductivity. For all metals in optical range: $\sigma/\omega >> 1$. The longitudinal component of the TR wave propagating inside metal along the electron motion (z axis) is proportional to $exp[i \cdot Kz]$, [7], where K the complex wave number: $K = k\sqrt{\varepsilon_m}$; k is the wave number in vacuum. Substitution from (6) gives: $K \approx k\sqrt{\frac{2\pi\sigma}{\omega}} \cdot (1+i)$. Because of the last item in the brackets the amplitude of the TR wave, caused by transition of electron through the boundary vacuum-metal, drops very rapidly and propagation of the TR wave in metal is limited by the skin-layer. At the same time the forward TR for the electron crossing the metal-vacuum boundary is calculated using the expressions (3). The backward TR for the electron crossing the vacuum-metal boundary is calculated using following expression, [8]:

$$I_B(\omega,\theta) = \frac{e^2\beta^2 \sin^2(\theta)\cdot\cos^2(\theta)}{\pi^2 c[1-\beta^2\cos^2(\theta)]^2} \cdot \left| \frac{(\varepsilon-1)\cdot(1-\beta^2+\beta\sqrt{\varepsilon-\sin^2(\theta)})}{(1+\beta\sqrt{\varepsilon-\sin^2(\theta)})\cdot(\varepsilon\cos(\theta)+\sqrt{\varepsilon-\sin^2(\theta)})} \right|^2 . \qquad (7)$$

An effect of the multiple scattering of the 16 MeV electrons in the 10 μm-thick single Mylar film varies the intensity in the total forward wave by few percent. This leads to insignificant blurring of the angular distribution of the OTR intensity. The effect drops with increasing of the electron energy. In considered energy range 16 MeV≤ E ≤250 MeV the multiple scattering in thin single film does not noticeably disturb the angular distribution of the forward OTR.

OTR Interferometry using two films with normal incidence of the electrons

The setup for the OTR interferometry (OTRI) at the A0 Photo injector was developed in three versions. In all of them two thin films are used as the OTRI source.

The first version of setup employs both transparent films displaced by a distance *D* with normal incidence of the electron beam. The forward OTR waves generated in both films (**A** and **B**) by one passing electron are detected through reflection in the mirror having a hole with size large enough for beam passage. The hole allows the scattered electrons to pass without noticeable OTR emission on the mirror. Note, that the hole changes the integral intensity of the interference pattern but does not change character of interference pattern because the OTRI light receiver (ICCD camera) is assumed to be focused on infinity.

The OTRI setup in plane of incidence is shown in Fig. 3. The θ_s is the projection of the r.m.s. angle of the multiple scattering for electrons passing through the first film.

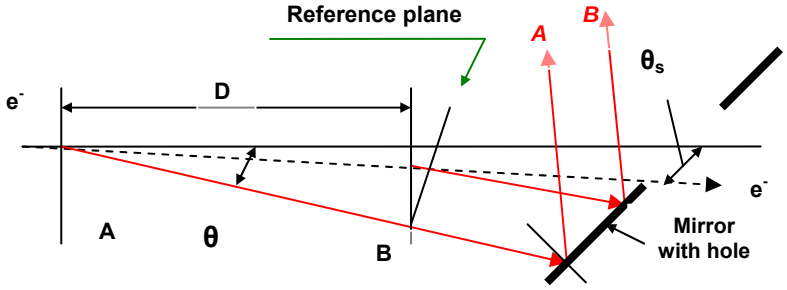

Fig. 3. OTRI setup with normal incidence of the beam. OTR waves ***A*** and ***B*** shown by red color caused by one electron passing through both films (**A** and **B,** shown by black color) interfere one with other.

The interference of OTR waves generated on **A** and **B** films installed with a displacement *D* was calculated using following expressions:

$$F_{TA}(\theta) = \left(F_I(\theta) + F_{II}(\theta)\right)\cdot \exp\left(i\cdot \Phi_A(\theta)\right), \quad (8)$$

$$F_{TB}(\theta) = \left(F_I(\theta) + F_{II}(\theta)\right)\cdot \exp\left(i\cdot \Phi_B(\theta)\right). \quad (9)$$

Here: $F_{TA}(\theta)$ describes total field in the forward OTR wave generated by crossing of the **A** Mylar film, $F_{TB}(\theta)$ describes the total field in the forward OTR wave generated by crossing of **B** film. $\Phi_A(\theta) = \dfrac{2\pi\cdot D}{\lambda\cdot\cos\theta}$ and $\Phi_B(\theta,\theta_s) = \dfrac{2\pi\cdot D}{\lambda}\left(\dfrac{1}{\beta\cdot\cos\theta_s} + (\tan\theta - \tan\theta_s)\cdot\sin\theta\right)$ are phases of the interfering waves ***A*** and ***B***, respectively, relatively to the reference plane. The expressions determine D to get the required fringes order, η: $\left|\Phi_A(\theta) - \Phi_B(\theta,\theta_s)\right| = \eta\cdot\pi$. This expression at $\theta_s << \theta$ gives following estimation for D: $D \geq \lambda/\left(\theta^2 + \gamma^{-2}\right)$.

Additionally one can consider the forward OTR generated by passage of electrons through **A** film, then reflected back on the **B** film and reflected again forward on **A** film:

$$F_{AR}(\theta) \approx r^2\left(1-r^2\right)\cdot F_{TA}(\theta)\cdot \exp\left(i\cdot\frac{4\pi\cdot D}{\lambda\cdot\cos\theta}\right), \tag{10}$$

and the backward OTR generated by passage of electrons through **B** film, and reflected forward on the **A** film:

$$B_{BR}(\theta) \approx r(1-r^2)\cdot\sqrt{I_B(\theta)}\cdot\exp\left[i\cdot\frac{2\pi\cdot D}{\lambda}\left(\frac{1}{\cos\theta_s}+\frac{2}{\cos\theta}\right)\right], \tag{11}$$

$$I_T(\theta) \approx \left|F_{TA}(\theta)+F_{TB}(\theta)+F_{AR}(\theta)+B_{BR}(\theta)\right|^2. \tag{12}$$

Here: $I_T(\theta)$ is the intensity of the interfering waves. Note that the total wave's fields include superposition of the multi-reflected forward waves in **A** film and multi-reflected forward waves in the film **B** as well.

Contribution of the last two items in (12) is quite low for films traditionally used for OTRI because of low value of the reflection coefficient. The calculated intensities of the interfering waves $I_T(\theta)$ at $\theta_{ms}=0$ and various thickness of Mylar are plotted in Fig. 4. For comparison intensities of superposition of the forward waves $I_F(\theta)=\left|F_{TA}(\theta)+F_{TB}(\theta)\right|^2$ and the intensity in the forward wave $I_{TA}(\theta)=\left|F_{TA}(\theta)\right|^2$ vs. θ are plotted as well.

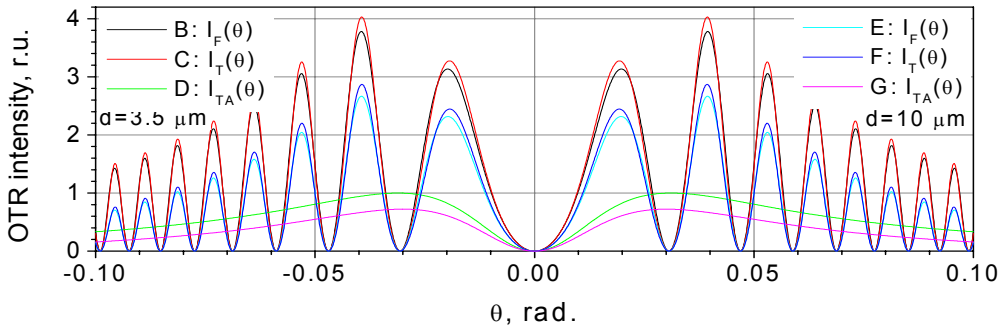

Fig. 4. Calculated distribution of the intensity in interfering waves generated in both: 3.5 μm or 10 μm Mylar films at λ = 0.632 μm for non scattered 16 MeV electrons. D = 1 mm.

Comparison of the interferograms first of all shows that film thickness (for non-scattered electrons) affects the fringes amplitude. Location of the fringes maxima and minima does not depend on the thickness for micrometers-thick considered films. Contributions of the backward wave from **B** film and the forward wave from **A** film reflected by **B** film one can omit in approximate calculations. Note that superposition of forward OTR waves generated by one boundary in each film at normal incidence of the beam (for non-scattered electrons) is acceptable for calculation of the angular radius of the fringes, but not for the amplitude.

Unlike the case of the single thin film in the two-film interferometer with the base length $D >> d$, the multiple scattering of the electrons in the **A** film strongly affects the interferogram. The effect was calculated assuming Gaussian distribution of the scattered angles for the multiple scattering of the electrons passing through the interferometer. For a distribution l of scattering angles θ_{sl} the partial intensities in the interfering waves were calculated. The common intensity was calculated as a sum of partial intensities at various scattering angles θ_{sl} considering the corresponding probabilities η_l of the scattering angle.

In the calculation for each angle θ_{sl} set of expressions similar to expressions (8)-(10) was used. Moreover we considered the bandwidth of a filter used to select the required wavelength:

$$F_{STA}(\theta,l,\lambda) = \left(F_I(\theta,\lambda) + F_{SII}(\theta,l,\lambda)\right)\cdot \exp\left(i\cdot\frac{2\pi\cdot D}{\lambda\cdot\cos\theta}\right), \quad (13)$$

$$F_{STB}(\theta,l,\lambda) = \left(F_I(\theta,\lambda) + F_{SII}(\theta,l,\lambda)\right)\cdot \exp\left[i\cdot\frac{2\pi\cdot D}{\lambda}\left(\frac{1}{\beta\cos\theta_{sl}} + (\tan\theta - \tan\theta_{sl})\sin\theta\right)\right], \quad (14)$$

$$I_{E16}(\theta) \approx \sum_{\lambda}\sum_{l}\left(\eta_l\cdot\left|F_{STA}(\theta,l,\lambda) + F_{STB}(\theta,l,\lambda)\right|^2\right). \quad (15)$$

Here: $F_I(\theta,\lambda)$ is expressed by (2), the subscript S means consideration of the multiple scattering. The subscript $E16$ in the resulting value of the intensity distribution points at the energy of electrons; summing over λ means summing over the filter bandwidth of ±0.005 μm with a center of 0.632 μm,

$$F_{SII}(\theta,l,\lambda) = \sqrt{I_{II}(\theta)}\cdot\exp\left[\frac{i\cdot 2\pi\cdot d}{\lambda}\left(\frac{1}{\beta\cos\theta_{sl}} + (\tan\theta_{\varepsilon} - \tan\theta_{sl})\sin\theta\right)\right].$$

The one dimensional projection of the r.m.s multiple scattering angle in the film with the thickness d was calculated using following expression, [10]:

$$\theta_s = \sqrt{\left\langle\theta_0^2\right\rangle} \cong \frac{13.6MeV}{\beta\cdot cp} z\cdot\sqrt{\frac{x}{X_0}}\cdot\left[1 + 0.038\ln\left(\frac{x}{X_0}\right)\right], \quad (16)$$

where: $x = \rho\cdot d$, ρ is the film density, X_0 is the radiation length of the film material.

The expression underestimates contribution of the scattering by big angles in comparison with method based on the Moliere theory and applicable for multiple scattering of the relativistic electrons, [11]. Fig. 5 shows the scattering angles for our film thickness range and the comparison of the two theories. However, OTR photons for the discussed energy range are radiated mainly with small angles. Because of that the described OTRI setups practically do not allow contribution of the OTR photons radiated by the electrons scattered by big angles. This will noticeably decrease the angles of the scattering determined using the OTRI setups and such phenomenon was observed, [2].

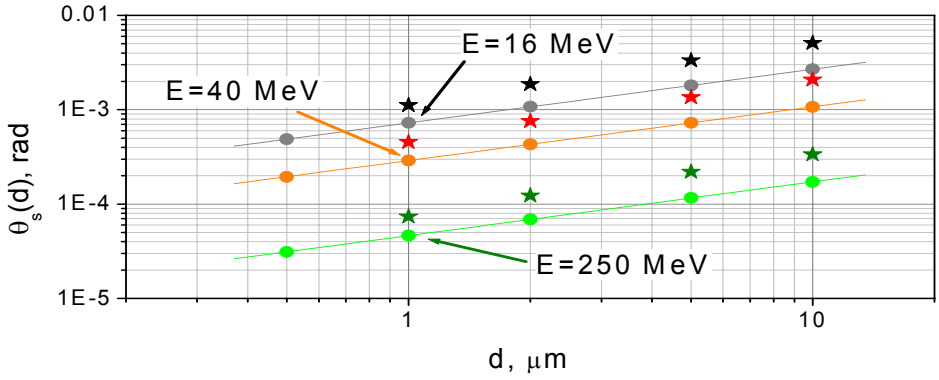

Fig. 5. Calculated values of the r.m.s. multiple scattering angles in a plane vs. the Mylar film thickness for different energy of electrons. Dots and lines show result obtained using expression (14); stars show results following from [10].

We calculated the OTRI pattern for 16 MeV, 40 MeV, and 250 MeV electrons passing through two 3.5 or 10 μm-thick Mylar films displaced by distance D considering multiple scattering of the electrons in the films and the filter bandwidth using the expressions (13-(16). Calculated the OTRI pattern profiles are presented in following figures. Calculated values of the θ_s for corresponding film thickness are presented in the figures as well.

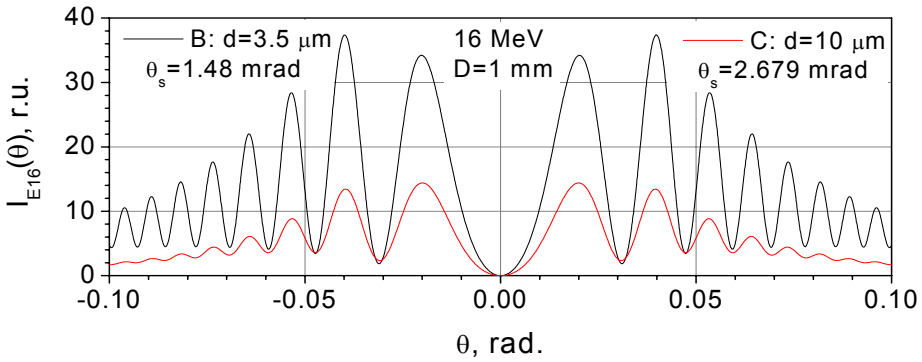

Fig. 6. OTRI pattern profiles considering multiple scattering for 16 MeV electrons passing through 3.5 μm or 10 μm -thick Mylar films at normal incidence of the electrons.

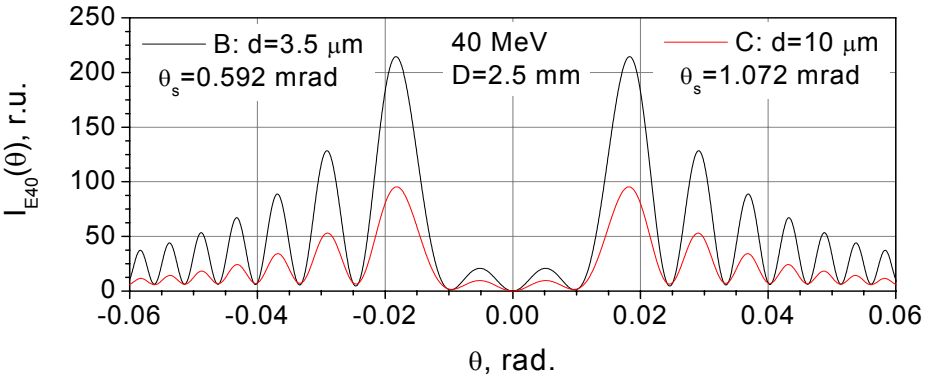

Fig. 7. OTRI pattern profiles considering multiple scattering for 40 MeV electrons passing through 3.5 μm or 10 μm -thick Mylar films at normal incidence of the electrons.

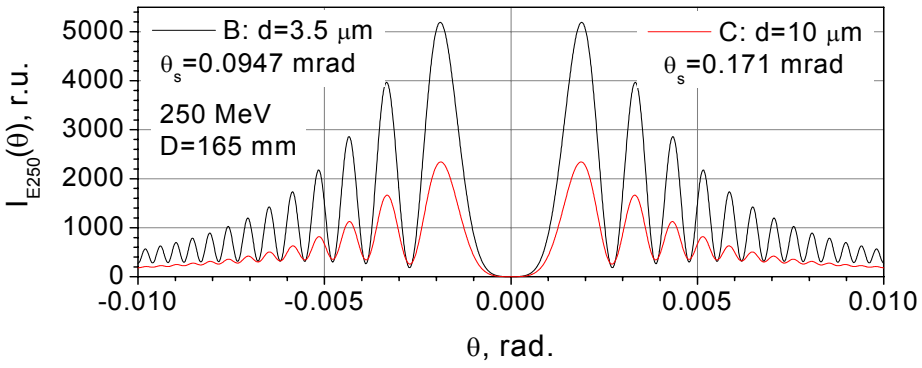

Fig. 8. OTRI pattern profiles considering multiple scattering for 250 MeV electrons passing through 3.5 μm or 10 μm -thick Mylar films at normal incidence of the electrons.

In the calculation we did not consider energy losses of the electrons in the films. The relative energy losses are less than 0.1% for the considered energy values and film thicknesses.

From the figures it follows that for multiple scattered electrons a decrease of the film thickness increases visibility (contrast) of the fringes, but does not change positioning of the fringes maxima and minima for considered values of the beam energy and the film thickness. The visibility ν is determined as: $\nu = (I_{\max} - I_{\min})/(I_{\max} + I_{\min})$; where: I_{max}, I_{min} are intensities in maximum and minimum of the fringes, respectively. Presented diagrams show noticeable range of variation of the visibility caused by variation of the projection of r.m.s. multiple scattering angle in the film. It makes possible application of the method in the diagnostics of the angles in the beam, [2].

OTR Interferometry using two films with 45^0 incidence of the electrons

This setup one can realize in following versions:

A). The first film is transparent; second one is mirror-reflecting, coated by metal; planes of films are parallel.

The setup in plane of incidence is shown in Fig. 9. The particle velocity ***β*** has the angle of $\psi = \pi/4$ with the normal ***z*** to the film plane in the point of incidence.

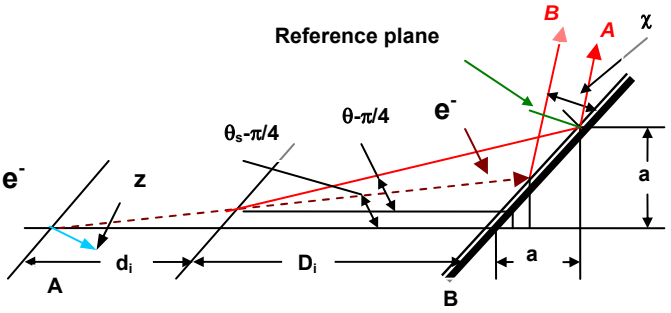

Fig. 9. Layout employing transparent film (**A**) and mirror-reflecting film (**B**) at the oblique incidence of the particles. For OTR TM and TE waves the electric field vectors are in plane of this figure and perpendicular to the plane, respectively. The **A** film thickness is shown magnified.

Note that for Mylar the total internal reflection angle $\theta_r = \mathrm{asin}(1/n) \approx 0.65$ *rad.*, so the main portion of the forward OTR generated on the entrance in the **A** film having $\pi/4 = 0.78$ *rad.* inclination to the beam axis disappears. Only the photons radiated with relatively big negative angles ≤ -0.1 rad contribute to the total forward OTR; their contribution drops very rapidly with increased energy of the electrons. For the energy of 16 MeV the contribution is approximately a few percents and one can omit it in the forward radiation generated by electrons passing through the **A** film in this energy range.

Intensity in the forward OTR TM wave generated on the second boundary of the **A** dielectric film is described by expression derived by V. Pafomov, [12]:

$$I_{FdTM}(\theta,\varphi,\omega) = \frac{e^2\beta_z^2 \cdot \cos^2\theta_z \cdot |1-\varepsilon|^2}{\pi^2 c\left[(1-\beta_x\cos\theta_x)^2 - \beta_z^2\cos^2\theta_z\right]^2 \sin^2\theta_z} \times$$

$$\times \left| \frac{(1-\beta_z\sqrt{\varepsilon-\sin^2\theta_z} - \beta_z^2 - \beta_x\cos\theta_x)\sin^2\theta_x + \beta_x\beta_z\cos\theta_x\sqrt{\varepsilon-\sin^2\theta_x}}{(1-\beta_x\cos\theta_x - \beta_z\sqrt{\varepsilon-\sin^2\theta_z})\cdot(\varepsilon\cos\theta_z + \sqrt{\varepsilon-\sin^2\theta_z})} \right|^2 . \qquad (17)$$

Here: $\varepsilon(\omega)$ is the permittivity of the dielectric film, θ is the angle between the normal to the film and wave vector of the OTR photon, $\beta_z = \beta\cos\psi$, $\beta_x = \beta\sin\psi$, ψ is the angle of incidence of the electrons; the directional cosines of the wave vector are determined as: $\cos\theta_x = \sin\theta\cdot\cos\varphi$; $\cos\theta_z = \cos\theta$.

The expression (17) has poles at $\theta \approx 0.223$ *rad.* and $\theta \approx 0.792$ *rad.* corresponding to the Cherenkov radiation. The first value is caused by the radiation lying on the Cherenkov cone at the negative angle refracted on the dielectric-vacuum boundary. One can exclude the radiation selecting angles significantly less than 0.223 rad for detection of the OTR.

Following [12] one can obtain intensity in the backward TM wave of the OTR, $I_{BmTM}(\theta,\varphi,\omega)$, on the boundary vacuum-metal of the **B** film. The expression differs from (17) by sign of β_z; instead permittivity of the dielectric must be used the substitution from (6).

Intensity in the TE component of the forward OTR generated on the boundary dielectric-vacuum is expressed as [12]:

$$I_{FdTE}(\theta,\varphi,\omega) = \frac{e^2\beta_x^2\beta_z^4\cdot\cos^2\theta_y\cdot\cos^2\theta_z\cdot|1-\varepsilon|^2}{\pi^2 c\left[(1-\beta_x\cos\theta_x)^2-\beta_z^2\cos^2\theta_z\right]^2\sin^2\theta_z}\times$$
$$\times\left|\left(1-\beta_x\cos\theta_x-\beta_z\sqrt{\varepsilon-\sin^2\theta_z}\right)\cdot\left(\cos\theta_z+\sqrt{\varepsilon-\sin^2\theta_z}\right)\right|^{-2}. \qquad (18)$$

Following [12], changing sign at β_z and using substitution for ε_m from (6), one can get expression for intensity of the TE component of the backward wave generated at the vacuum-metal boundary of the **B** film, I_{BmTE}.

The intensities of the TM and the TE OTR waves at $\psi = \pi/4$ are plotted in Fig. 10.

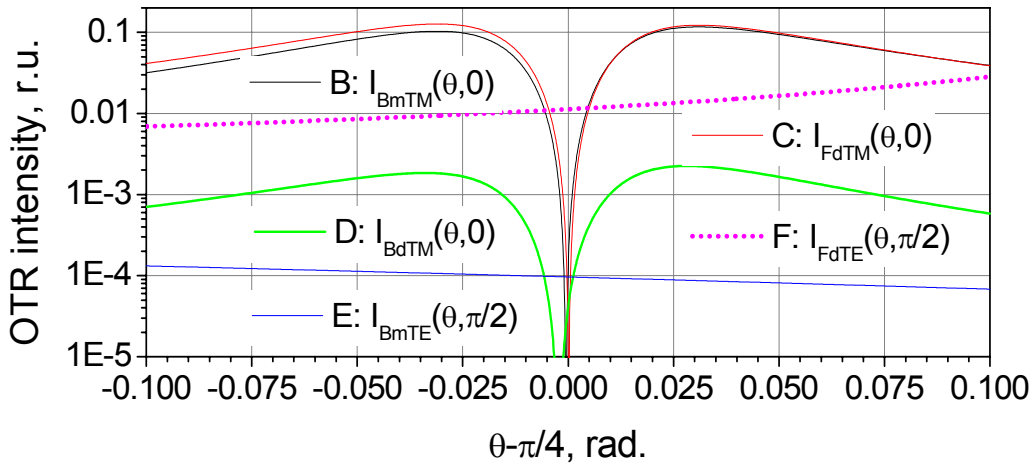

Fig.10. OTR TM waves intensities at the tilt angle of the OTR screen to the beam axis of 45^0.

In the figure is also plotted the intensity distribution in the backward TM wave, I_{BdTM}, from the boundary vacuum-Mylar. The intensity is only few percents relatively the intensity of the backward TM wave generated on the boundary vacuum-mirror-reflecting metal. The TM OTR I_{FdTM} distribution at 45^0 incidence of the electrons in amplitude practically coincides with OTR distribution caused by transition of electrons through the

boundary dielectric-vacuum (I_{II}, Fig. 2) at normal incidence. Note that the intensity distributions I_{FdTM} and I_{BmTM} are close one to other.

For described setup main contributions in the interference pattern are given by the TM component of the forward OTR wave generated on **A** (transparent) dielectric film and TM component of the backward OTR wave generated on the **B** film (mirror-reflecting metal), Fig. 10. Obviously the TE waves only at $\varphi \cong \pi/2$ will contribute to the interference with the considered TM waves. The contribution is noticeable at the angle $\theta \cong \pi/4$ as $I_{FdTM}(\pi/4,\varphi,\omega)=0$ and $I_{BmTM}(\pi/4,\varphi,\omega)=0$.

Based on noted above for simplified calculations we consider superposition of the forward OTR waves ($F_{ATM}(\theta)+ F_{ATE}(\theta)$) generated on second boundary of the **A** film:

$$F_A(\theta,\varphi)=\left(\sqrt{I_{FdTM}(\theta,\varphi)}+\sqrt{I_{FdTE}(\theta,\varphi)}\right)\cdot\exp\left[\frac{i\cdot 2\pi}{\lambda}\cdot\left[\frac{D_i}{\cos\alpha_s}\left(1+\frac{\tan\alpha}{1-\tan\alpha}\right)\right]\right], \qquad (19)$$

and the backward OTR waves, generated on the first boundary of the **B** metal-coated film:

$$B_B(\theta,\varphi)=\left(\sqrt{I_{BmTM}(\theta,\varphi)}+\sqrt{I_{BmTE}(\theta,\varphi)}\right)\cdot\exp\left[\frac{i\cdot 2\pi\cdot D_i}{\lambda}\cdot\left[\frac{1+\frac{\tan\alpha_s}{1-\tan\alpha_s}}{\beta\cos\alpha_s}+\sqrt{2}\left(\frac{\tan\alpha}{1-\tan\alpha}-\frac{\tan\alpha_s}{1-\tan\alpha_s}\right)\cdot\cos\chi\right]\right], \qquad (20)$$

Here: $D_i=\sqrt{2}\cdot D$; $\alpha_s=\theta_s-\pi/4$; $\alpha=\theta-\pi/4$; $\chi(\theta)=\pi/2-\theta$. The angular distribution of the intensity of the interfering waves is calculated as:

$$I_{iE16}(\theta,\varphi)\approx\left|F_A(\theta,\varphi)+B_B(\theta,\varphi)\right|^2. \qquad (21)$$

The calculated interference pattern profile in plane of incidence for non scattered electrons having energy of 16 MeV at λ = 0.632 μm is shown in Fig. 11. Note that the OTRI pattern profile for non-scattered electrons does not depend on the film thickness because of total internal reflection of the OTR generated on the entrance of the transparent film.

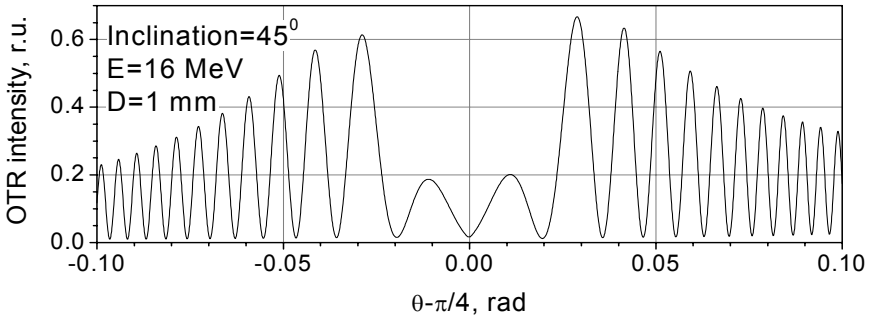

Fig. 11. E=16 MeV; D=1 mm; films inclination of 45^0; non scattered electrons.

Using the same method calculating of the multiple scattering effects in film **A** as was done above and summing the obtained results over the filter bandwidth we have computed distributions of the intensity in interfering waves for various **A** film thickness at the beam energy of 16 MeV, 40 MeV and 250 MeV. The computations were done at the distances between **A** and **B** films of 1 mm, 2.5 mm and 165 mm, respectively, and at λ=(0.632±0.005) μm. The following figures demonstrate the interference pattern profiles.

Note that for measurements with large value of D use of mirror-reflecting metal surface instead the first transparent film can be preferable.

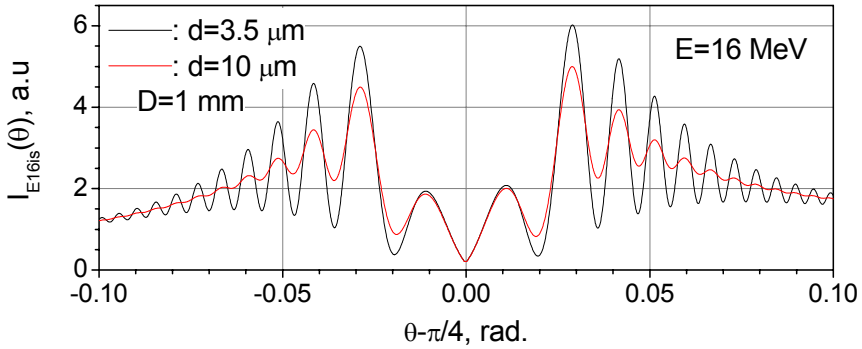

Fig. 12. E=16 MeV; d= 3.5 μm, 10 μm; D=1.0 mm; films inclinations are 45^0.

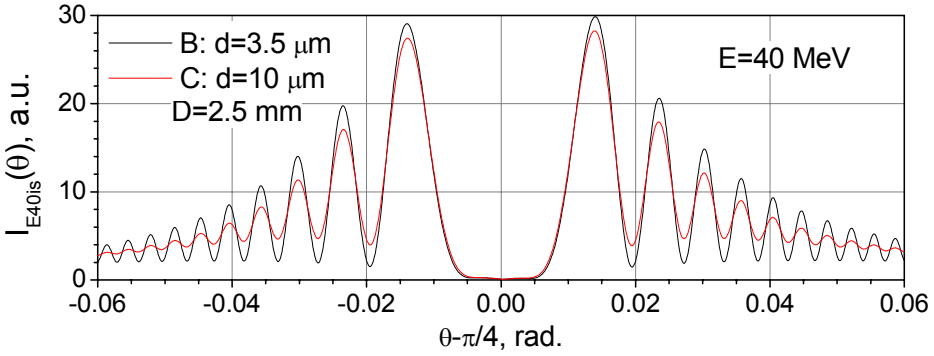

Fig. 13. E=40 MeV; d= 3.5 μm, 10 μm; D=2.5 mm; films inclinations are 45^0.

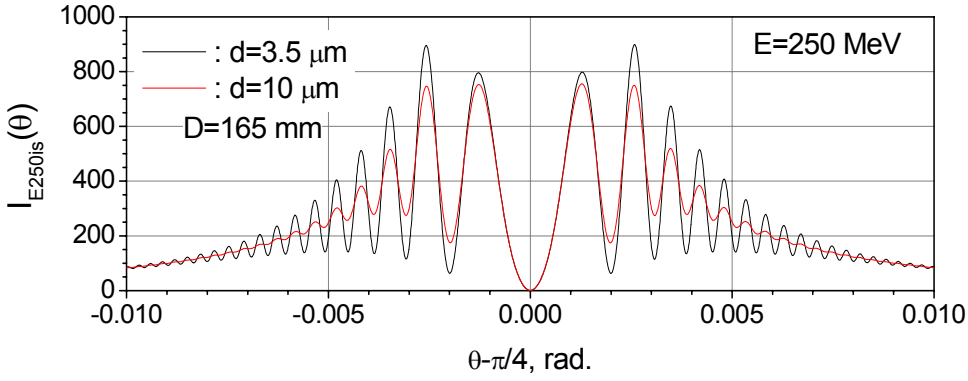

Fig.14. E=250 MeV; d= 3.5 μm; 10 μm, D=165 mm; films inclinations are 45^0.

The computed plots also demonstrate decreasing of the fringes visibility with increasing of the **A** film thickness because of the electron multiple scattering in the first film, so from point of view of minimization of the scattering, the normal inclination of the interferometer is preferable, but is needed in additional special mirror with hole. Note

that the value of intensity in the interference pattern for interferometer having the normal incidence is approximately in one order higher than that for interferometer having 45^0 inclinations of the films to the beam axis.

B). The OTR interferometer has both transparent films with inclination of *π/4 rad.* to the beam axis.

The layout in the plane of incidence is shown in Fig. 15. The optical scheme differs from that shown in Fig. 9. Here backward OTR from the **A** film has to be considered because the reflectivity of the transparent film **B** at this setup is quite low.

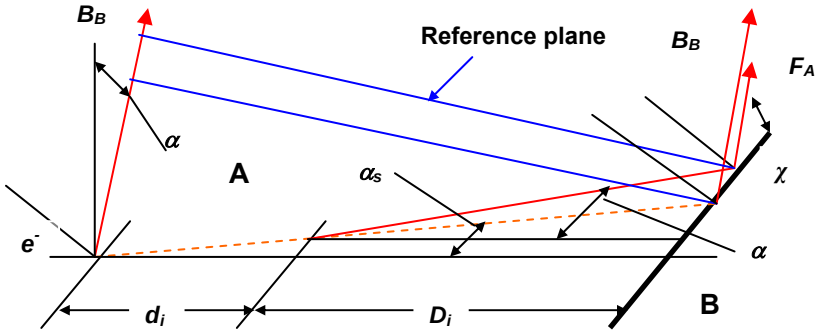

Fig. 15. Interferometry with both transparent films. The **A** film thickness is shown magnified.

For simplified calculation one considers superposition of the backward TM waves generated on the boundaries vacuum-dielectric in both films, $B_A(\theta,\phi)$ and $B_B(\theta,\phi)$, and the forward TM wave, $F_{Ar}(\theta,\phi)$ generated on the boundary dielectric-vacuum of the first film, reflected by **B** film.

$$B_A(\theta,\varphi) = \sqrt{I_{BdTM}(\theta,\varphi)} \cdot \exp(i \cdot \Phi_{AB}(\alpha,\alpha_e)), \tag{22}$$

$$B_B(\theta,\varphi) = \sqrt{I_{BdTM}(\theta,\varphi)} \cdot \exp(i \cdot \Phi_{BB}(\alpha,\alpha_e)), \tag{23}$$

$$F_{Ar}(\theta,\varphi) \approx \sqrt{I_{FdTM}(\theta,\varphi)} \cdot r_{TM}(\theta) \cdot \exp(i \cdot \Phi_{AF}(\alpha,\alpha_s)). \tag{24}$$

Here: $r_{TM}(\theta)$ is the reflection coefficient for the TM waves, [7]:

$$r_{TM}(\theta) = \frac{n^2\cos(\theta) - \sqrt{n^2 - \sin^2(\theta)}}{n^2\cos(\theta) + \sqrt{n^2 - \sin^2(\theta)}}, \tag{25}$$

The phases of the interfering TM waves relatively to the reference plane are expressed as:

$$\Phi_{AB}(\alpha,\alpha_s) = \frac{2\pi \cdot D_i}{\lambda}\left[\left(1 + \frac{\tan\alpha_s}{1-\tan\alpha_s}\right)\cdot\frac{\cos(\alpha+\alpha_s)}{\cos\alpha_s} + \sqrt{2}\left(\frac{\tan\alpha}{1-\tan\alpha} - \frac{\tan\alpha_s}{1-\tan\alpha_s}\right)\cdot\cos\chi\right],$$

$$\Phi_{BB}(\alpha,\alpha_e) = \frac{2\pi \cdot D_i}{\lambda}\left[\frac{1 + \frac{\tan\alpha_s}{1-\tan\alpha_s}}{\beta\cdot\cos\alpha_s} + \sqrt{2}\left(\frac{\tan\alpha}{1-\tan\alpha} - \frac{\tan\alpha_s}{1-\tan\alpha_s}\right)\cdot\cos\chi\right],$$

$\Phi_{AF}(\alpha) = \frac{2\pi \cdot D_i}{\lambda\cos\alpha}\left(1 + \frac{\tan\alpha}{1-\tan\alpha}\right)$. The angles: ψ, α, α_s, and χ were defined above.

The angular distribution of the interfering waves is:

$$I_{ti}(\theta,\varphi) \approx \left|B_A(\theta,\varphi) + B_B(\theta,\varphi) + F_{Ar}(\theta,\varphi)\right|^2. \tag{25}$$

The plot of the (total) intensity distribution in plane of incidence is shown in Fig. 16.

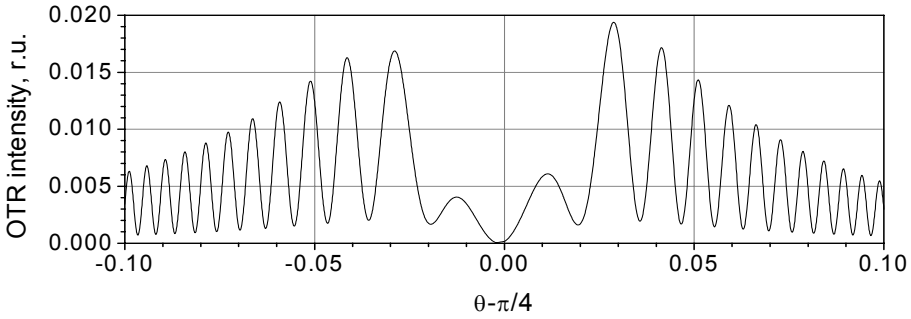

Fig. 16. E=16 MeV; D=1 mm; films inclination of 45^0; non scattered electrons.

The pattern shape in the figure is quite similar to the plot of the OTRI pattern for the interferometer using tilted by 45^0 transparent and mirror-reflecting films, Fig. 11, but the intensity is in 20-30 times less because of low reflectance of the Mylar uncoated films. The same remarks are valid to computations considering the multiple scattering of the electrons in **A** film. So the intensities in the interference patterns for the interferometer using both transparent films tilted to the beam axes by 45^0 are approximately two orders of magnitude less than those calculated for interferometer with normal incidence of the beam. Nevertheless the setup using both transparent films with inclination of 45^0 to the beam axes can be useful for the OTRI diagnostics at higher energies of the electrons (few tens of MeV or higher).

Application of the OTRI for the beam diagnostics at the A0 Photoinjector and the ILC Photoinjector prototype

OTR two-film interferometry is attractive as a diagnostics method for investigation of the beam parameters at A0 Photoinjector and the ILC prototype Photoinjector due to its unique properties in determination of the angles and the energy in the relativistic beam.

For the determination of the angles in the electron beam one can use the expressions derived above corresponding to the appropriate experimental setup. Assuming a Gaussian distribution in beam angle, [3], one can determine the mean-square beam angle $\left\langle \theta_b^2 \right\rangle$ through measurement of the mean-square total angle $\left\langle \theta_t^2 \right\rangle$ affecting the fringes visibility. Measuring the fringe visibility and correcting for the mean-square angle of the multiple scattering of the electrons in a film, $\left\langle \theta_s^2 \right\rangle$, the mean-square beam divergence angle can be determined:

$$\left\langle \theta_b^2 \right\rangle = \left\langle \theta_t^2 \right\rangle - \left\langle \theta_s^2 \right\rangle .$$

It is appropriate to measure the visibility of the fringes using pattern profiles in the range of angles of ~ $\pm(2\text{-}5)\cdot 1/\gamma$ and utilizing few firsts fringes. To get better accuracy in determination of the angles in the beam one needs to minimize the mean-square angle of the multiple scattering in the **A** film, i.e. one need to choose minimal thickness (and density) of the **A** film. In this case the setup with normal incidence of the beam and utilization of super thin low density **A** film is preferable. Good choice for the setup is

utilizing of the 0.5-5 μm commercial tensioned mirror-reflecting aluminum foil, [13], or tensioned Mylar film.

The simulated dependence of r.m.s. beam angle, $\theta_b(\nu) = \sqrt{\langle \theta_b^2(\nu) \rangle}$, on visibility for monoenergetic 16-MeV electron beam at the normal incidence of the electrons and d=1 μm (Mylar film) is shown in Fig. 17.

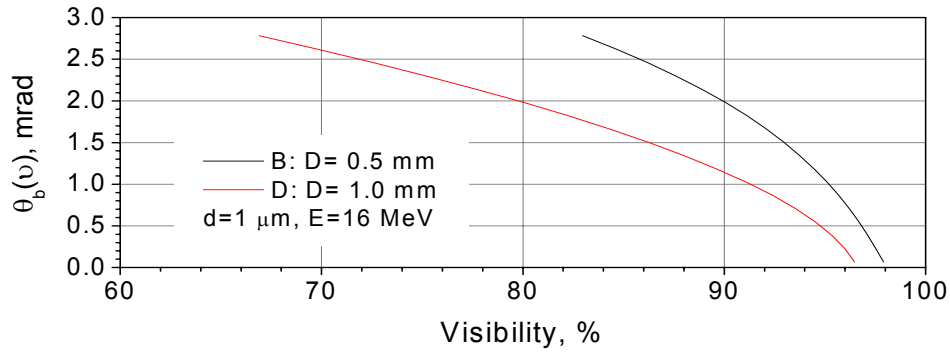

Fig. 17. Calculated angles in the beam vs. visibility for the OTRI pattern at normal incidence.

Fig. 17 shows that for investigation of small angles in the beam (≤ 1 mrad) is better to use bigger displacement; that gives more significant variation of the visibility per angle unit. At the angles ≥ 1 mrad smaller displacement provides wider range of the measured angles at the same range of visibility. I.e. the films displacement D has to be optimized for the measurements.

Note that the OTR screen thickness has a low limit depending on the electron energy. The limit is the formation length $l_f \approx \gamma \cdot c/\omega_p$, which is a distance required to reform electric field of the particle passing through the boundary of two medias accordingly to variation of the polarization properties of the medias. [14, 7]; that yields $d \geq 0.3\ \mu m$, $d \geq 0.8\ \mu m$, and $d \geq 5\ \mu m$, for the electron beam energy of 16 MeV, 40 MeV and 250 MeV, respectively. Use of smaller thicknesses of the films leads to cutoff of the TR frequency spectrum; that affects first of all the higher frequencies in forward TR.

Following from Fig. 5 the r.m.s. value of the scattering angle at $d = 0.5\ \mu m$ is ~ 0.5 mrad in Mylar film at the energy of the beam of 16 MeV. Measured value of the bean divergence at the charge of 4 nC and the energy of ~ 16 MeV for the A0 Photoinjector operating with the single laser pulse is in the range of 0.25-0.75 mrad, so one can expect that OTRI method should be useful to measure the angles in the beam at electron beam energy in the range of tens-hundreds MeV.

For relativistic electrons maximum of the OTR intensity corresponds approximately to the angle of radiation of $1/\gamma$. Because of this, one can use the angular distribution of the OTR to characterize the energy of the electron beam. OTRI significantly improves the resolution of the energy measurements. In Ref. [2] application of the developed OTRI method provided precision of the energy determination of ~ 1% at the energy of electrons in few tens MeV.

From the interferometer principle follows that increased distance D between films provides higher resolution of the energy measurements. The interference patterns at the measurements have to be observed at smaller angles than $1/\gamma$. Of course one has to

minimize the film thickness to get better visibility (and resolution of the method). Fig. 18 demonstrates calculated interference pattern profiles for a change of the beam energy by 1% at 16 MeV at various values of the displacement *D*. The calculation was done for the setup with normal incidence of the electrons and Mylar film thickness of d =1 μm.

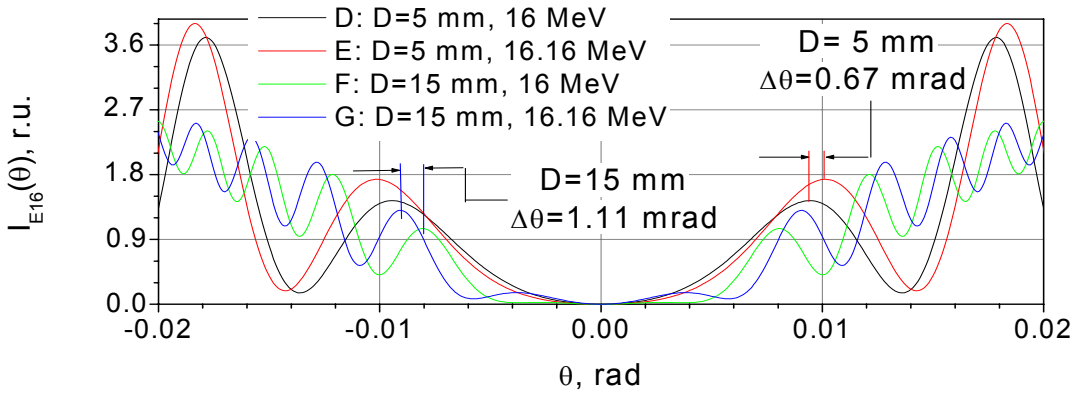

Fig. 18. The interference pattern profiles vs. the beam energy at different interferometer base *D*. Arrows show the difference in angular radius for first fringes at D=5 mm (plotted by red and black colors) and D=15 mm (second fringes; blue and green colors).

The figure shows increase in angular difference of the fringes, $\Delta\theta$, at increase of the base *D*: at variation of the beam energy by 1 % the difference is increased from 0.67 mrad. to 1.11 mrad. by changing the *D* value from 5 mm to 15 mm. However increase of the base concurrently leads to a decrease of the fringes visibility. Fig. 19 shows how the angular radius and visibility are changing with D value.

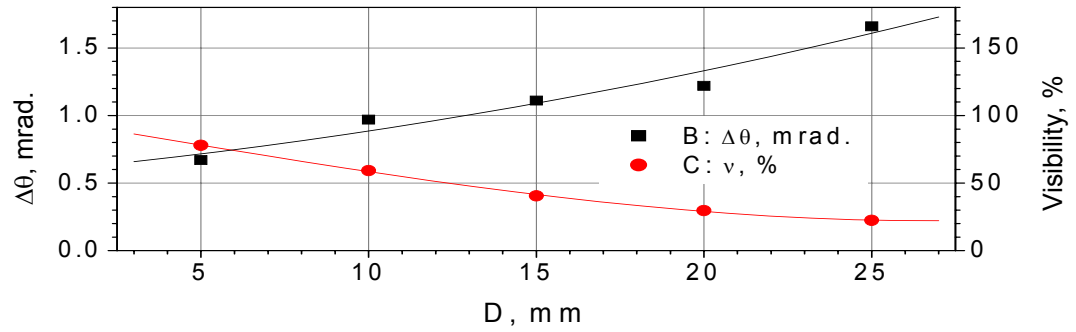

Fig. 19. Calculated angular difference Δθ and visibility of the fringes vs. the interferometer base D at the beam energy increase by 1 % and Mylar film thickness of 1 μm.

Optimizing the interferometer base *D* and choosing an appropriate corresponding focal length of the camera objective one can provide required space resolution of the pattern. Note that the beam energy spread causes blurring of the fringes. Moreover the shape of the electron beam energy spectrum affects the position of the fringes maxima and minima. Fig. 20 shows difference in the calculated OTRI pattern profiles for 16-MeV monoenergetic electrons compared with the beam of 16 MeV with FWHM ~ 0.4% in the energy spread (conditions similar to those at A0 Photoinjector). Computation of the OTRI pattern profile for the beam having energy spread was done via summation over all values of energy in the beam spectrum.

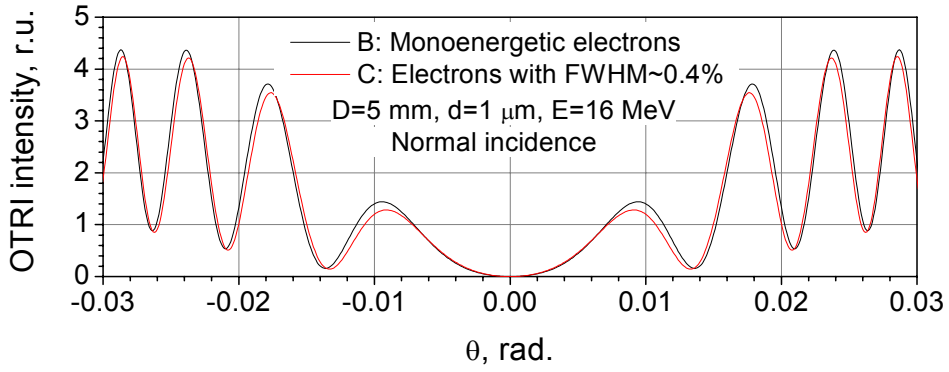

Fig. 20. OTRI pattern profiles for 16-MeV mono energetic electrons and the beam with FWHM ~ 0.4 % in the energy distribution.

Decrease of the angular radius of the fringes for non-monoenergetic beam, Fig. 20, is caused by displacement of the gravity center in the energy spectrum of the electrons to lower energy because of the tail of the beam. For lower energy of the electrons generating the OTR the phase shift in interfering waves is bigger, so the fringes radius is smaller. This effect one can see in Fig.2 and in Fig. 18 as well.

Summary

In the report we considered various OTRI experimental setups and developed simulations for the OTR interferometry at A0 Photoinjector. Preparation of the setups for experimental check now is in progress. Presented simulations should be compared with measured results.

References

[1] V.L Ginzburg and I.M. Frank, J. Exp. and Theoret. Phys., Vol. 16, pp. 15-21, 1946.
[2] L. Wartski et al., J. of Appl. Phys. Vol. 46, No. 8, 3644-3653, 1975.
[3] R.B. Fiorito and D.W. Rule, AIP Conference Proceed. Beam Instrumentation Workshop, V. 319, pp. 21-37, 1994.
[4] R.B. Fiorito and A.G. Shkvarunets, Proceedings DIPAC 2003, pp. 89-91, 2003.
[5] D.W. Rule et. al., NIM A296, (1990), 739-743,
[6] V.L Ginzburg and V.N. Tsytovich, Physics reports, 49 no. 1, pp.1-89, 1979.
[7] J.D. Jackson, Classical electrodynamics, Wiley, New York, 1999.
[8] L.D. Landau and E.M. Lifshitz, Electrodynamics of continues media, Addison-Wesley, 1960.
[9] L.A. Vainstein, Electro-magnetic waves, Radio & Communication, Moscow, 1988.
[10] Review of Particle Physics, Phys. Rev. D, V 54, No 1, 132-139, 1996.
[11] Alfa, beta and gamma-ray spectroscopy, Edited by K. Siegbahn, North-Holland, Amsterdam, 1965.
[12] M.L. Ter-Mikaelian, High-Energy Electromagnetic Processes in Condensed Media, Wiley-Interscience, New-York, 1972.
[13] V. Scarpine, Private communication.
[14] G.M. Garibyan, Sov. Phys. JETP 6, 1079, 1958.